RSC Advances

PAPER

View Article Online
View Journal | View Issue

Cite this: *RSC Adv.*, 2024, **14**, 21151

Rapid synthesis of aminal-linked covalent organic frameworks for CO_2/CH_4 separation†

Jianwei Yang, Xianghao Han* and Xiao Feng *

Received 2nd April 2024
Accepted 20th June 2024

DOI: 10.1039/d4ra02505a

rsc.li/rsc-advances

As an emerging category of crystalline porous materials, covalent organic frameworks (COFs) are primarily synthesized *via* solvothermal methods. However, achieving rapid synthesis of COFs through this approach poses a significant challenge. To address the issue of slow synthesis, we studied the crystallization process of aminal-linked COFs *via* the condensation of a cost-effective aldehyde and secondary amine, and successfully expedited the synthesis of COFs within a one-hour duration. Furthermore, gram-scale aminal-linked COFs with abundant ultra-microporous channels demonstrated promising potential for CO_2/CH_4 separation. This study enables the rapid synthesis of aminal-linked COFs from cheap raw materials, which lays a foundation for their practical applications.

Introduction

Covalent organic frameworks (COFs) are an emerging class of crystalline porous materials constructed by stitching organic building units together with covalent bonds, featuring advantages such as low density, designable structures, and facilely tailored functionalities.[1–3] These unique attributes endow COFs with exceptional potential for a wide range of applications in adsorption,[4–6] separation,[7,8] catalysis,[9–13] sensing,[14,15] drug delivery,[16–18] energy storage,[19–21] and so on. Since the pioneering work reported by Yaghi and co-workers in 2005,[1] this field has undergone a rapid expansion over the past decade. The formation of crystalline COFs primarily entails a dynamic "self-healing/error-correction" process facilitated by reversible covalent bonds.[22,23] This process typically requires high energy input and prolonged reaction durations to drive the reversible process to form thermodynamically stable crystalline products. For instance, the widely used solvothermal method employed for COF synthesis often spans several days or even months.[24,25] However, the lengthy reaction times, complex procedures, and high energy consumption associated with this method hinder the functionalization and industrial application of COFs. Efforts to achieve simple and rapid synthesis approaches have long persisted, with various alternative energy sources, including microwave,[26,27] ultrasound,[28,29] mechanical agitation,[30,31] light irradiation,[32] and electron beam,[33] have been utilized to substantially shortened reaction times from multiple days to several hours, and even seconds in extreme cases. Moreover, the optimization of the reaction system (such as solvent, catalyst, temperature, *etc.*) holds promise for expediting COF formation by accelerating the bond formation and enhancing the error correction process during the crystallization process.[34–36] However, these endeavors mainly concentrated on specific types of COFs, while the utilization of alternative energy sources frequently entails the procurement of costly equipment and adherence to stringent operational protocols. Hence, it is necessary to develop feasible and practical new methods and new materials to rapidly synthesize COFs.

It is well known that the aminal linker is a very promising linkage because of its good reversibility, which is comparable to that of the imine bond.[37,38] This property enables facile dynamic structural adjustment and defect repair, making aminal linker the promising candidates for rapid synthesis of highly crystalline COFs. Nevertheless, this field remains relatively

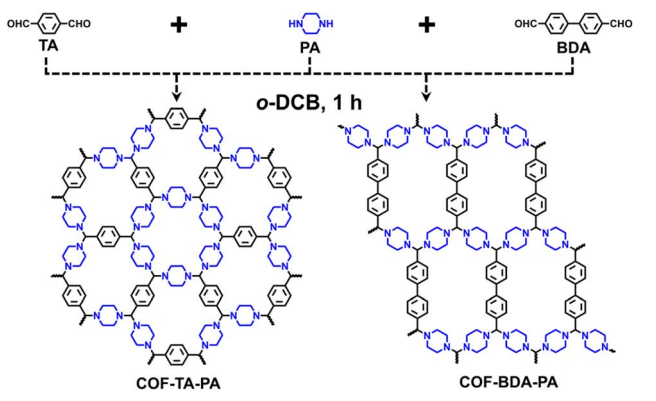

Scheme 1 Synthetic scheme of COF–TA–PA and COF–BDA–PA *via* solvothermal methods.

Beijing Key Laboratory of Photoelectronic/Electrophotonic Conversion Materials, Key Laboratory of Cluster Science, Ministry of Education, Advanced Technology Research Institute (Jinan), Frontiers Science Center for High Energy Material, School of Chemistry and Chemical Engineering, Beijing Institute of Technology, Beijing, China. E-mail: fengxiao86@bit.edu.cn; hanxh5@126.com

† Electronic supplementary information (ESI) available. See DOI: https://doi.org/10.1039/d4ra02505a

underexplored with only five reported instances since the first pioneering work reported by Zhao in 2019.[37,39,40] This scarcity and unknown attract our attention and prompt us to explore the properties of aminal-linked COFs. Hence, in this study, we mainly focused on exploring the feasibility of rapid synthesis of aminal-linked COFs.

To realize the above idea, we chose readily available and cost-effective terephthalaldehyde (TA, $23 per kg) and piperazine (PA, $18 per kg) as monomers to study the crystallization process of aminal-linked COFs (COF–TA–PA, Scheme 1). We used powder X-ray diffraction (PXRD) patterns and Brunauer–Emmett–Teller (BET) surface areas, which were acquired under uniform data collection parameters, as a benchmark to evaluate the growth of COFs synthesized under different conditions.

Experimental

Materials

All the chemicals commercially available were used directly without further purification. TA, 4,4′-biphenyldicarboxaldehyde (BDA), and PA were purchased from Energy Chemical. Glacial acetic acid, mesitylene (Mes), toluene (Tol), 1,4-dioxane (Dio), and *o*-dichlorobenzene (*o*-DCB), dimethylacetamide (DMAc), and *n*-butanol (*n*-BuOH) other common solvents were purchased from Energy Chemical and Sigma-Aladdin.

Synthetic procedures

Synthetic of COF–TA–PA. A 10 mL Pyrex tube was charged with TA (134 mg, 1 mmol) and PA (258 mg, 3 mmol). Then *o*-DCB (5 mL) was added and the mixture was sonicated for 10 min to get a homogeneous dispersion. The tube was degassed under vacuum and then sealed. The ampoule was warmed to room temperature and then kept at 120 °C without disturbance for 12 h. After being cooled to room temperature, the precipitate was collected through filtration, followed by washing three times with anhydrous THF. The resulting product was further purified by using Soxhlet extraction in anhydrous THF and then dried at 90 °C for 6 hours under a dynamic vacuum to afford a yellow powder (265 mg, 98% yield). Anal. calcd for $C_{16}H_{22}N_4$: C, 71.08; H, 8.20; N, 20.72. Found: C, 70.54; H, 8.17; N, 19.69.

Gram-scale synthetic of COF–TA–PA. A 50 mL Pyrex tube was charged with TA (1.34 g, 0.01 mol) and PA (2.58 g, 0.03 mol). Then *o*-DCB (30 mL) was added and the mixture was sonicated for 10 min to get a homogeneous dispersion. The tube was degassed under vacuum and then sealed. The ampoule was warmed to room temperature and then kept at 120 °C without disturbance for 12 h. After being cooled to room temperature, the precipitate was collected through filtration, followed by washing with THF. The resulting product was further purified by using Soxhlet extraction in anhydrous THF and then dried at 90 °C for 6 hours under a dynamic vacuum to afford a yellow powder (2.23 g, 83% yield). Anal. calcd for $C_{16}H_{22}N_4$: C, 71.08; H, 8.20; N, 20.72. Found: C, 70.17; H, 8.21; N, 19.38.

Synthetic of COF–BDA–PA. COF–BDA–PA was synthesized following the same procedures as COF–TA–PA except for the kinds of reactants BDA ((210 mg, 1 mmol) and PA (258 mg, 3 mmol)). The post-processing operations were the same as above. Finally, a yellow powder was obtained (312 mg, 90% yield). Anal. calcd for $C_{22}H_{26}N_4$: C, 76.27; H, 7.56; N, 16.17. Found: C, 75.39; H, 7.70; N, 14.75.

Gram-scale synthetic of COF–BDA–PA. Gram-scale COF–BDA–PA was synthesized following the same procedures as gram-scale COF–TA–PA except for the kinds of reactants (BDA (2.10 g, 0.01 mol) and PA (2.58 g, 0.03 mol)). The post-processing operations were the same as above. Finally, a yellow powder was obtained (312 mg, 90% yield). Anal. calcd for $C_{22}H_{26}N_4$: C, 76.27; H, 7.56; N, 16.17. Found: C, 74.59; H, 7.55; N, 15.15.

Characterization

Powder X-ray diffraction analyses were performed using a Rigaku MiniFlex 600 diffractometer operating at 40 kV voltage and 15 mA current with Cu-Kα X-ray radiation (λ = 0.154056 nm) with a step size of 0.02° in 2θ from 1.5 to 30°. Fourier transform infrared (FT-IR) spectra were collected in the range of 450–4000 cm^{-1} on Bruker ALPHA spectrometer equipped with an ATR cell. Solid state ^{13}C CP-MAS nuclear magnetic resonance (NMR) spectroscopy was carried out on an Agilent DD2 spectrometer operating at 150.78 MHz for ^{13}C. A double resonance 4 mm T-3 MAS probe was used for all the experiments. The ^{13}C CP/MAS spectra were acquired using a tancpxtoss sequence, with a contact time of 1 ms and a recycle interval of 2 s. The spinning rate was set to 8 kHz. Nitrogen sorption measurements were performed on Quantachrome Instrument ASiQMVH002-5. The isotherms were collected from 0 to 1 atm at 77 K under liquid nitrogen bath. The Brunauer–Emmett–Teller (BET) method was utilized to calculate the specific surface areas. By using the quenched-solid density functional theory (QSDFT) model, the pore size distribution profile was derived from the adsorption data. Field-emission scanning electron microscopy (SEM) images were acquired from a JEOL model JSM-7500F scanning electron microscope. High-resolution transmission electron microscopy (TEM) was performed on an FEI Tecnai G2 F30. X-ray photoelectron spectroscopy (XPS) was performed using a Thermo Scientific K-Alpha$^+$ monochromatic Al K-α source with an electron emission angle of 0 degrees. The analysis region was a circle with a diameter of 400 μm. The work function (ΦSA) of COFs is marked as 4.84 eV,[41] so the calculated C 1s peak (E_B = 289.58 − ΦSA)[42] is 284.74 eV as the internal standard. Thermal gravimetric analyses (TGA) were carried out on the Netzsch STA449F5 analyzer by heating the samples from 25 to 800 °C under nitrogen atmosphere at a heating rate of 10 °C min^{-1}. Elemental analysis was performed on a Thermo FLASH 2000.

Static adsorption and breakthrough tests

The static CO_2 and CH_4 sorption isotherms were conducted on Belsorp Max II at 273, 283, and 298 K. The breakthrough separation experiments were conducted in a home-built breakthrough apparatus under ambient conditions (298 K, 1 atm). The separation of CO_2/CH_4 was carried out in a fixed bed. Aminal-linked COFs (1.0 g) were packed in a stainless column

(6 mm inner diameter, 200 mm length) and purged with He flow (20 mL min^{-1}) for 0.5 hours at 298 K for the activation process. Meanwhile, as a carrier gas, the He was also used to clean the system. The flow rate (2.0 mL min^{-1} at 298 K and 1 atm) of CO_2/CH_4 with volume rations of 50/50 was regulated by mass flow controllers. Outlet gas from the sample holder was monitored by using chromatography (GC-9860-5C-NJ). After the breakthrough experiment, the adsorbent was *in situ* regenerated by flowing He for 30 min at 298 K to finish three cycles of the experimental breakthrough tests.

Results and discussion

Initially, we examined the influence of solvents on the crystallinity of COF materials. To this end, COF–TA–PA was prepared in eight different solvents without Lewis acid catalysts, and the condensation reaction was carried out in a sealed tube at 120 °C for 3 days. After work-up, the PXRD patterns of the as-obtained products were recorded. As shown in Fig. 1, crystalline COF–TA–PA was obtained not only in monophasic organic solvent systems (*e.g.*, Mes, Tol, Dio, and *o*-DCB), but also in a range of mixed solvent compositions such as Mes/*n*-BuOH, Mes/Dio, DMAc/Mes, and DMAc/Tol (Table S1†). Experimental findings indicate exceptional solvent adaptability of COF–TA–PA, with a preference observed for the *o*-DCB system, which is different from previously reported aminal-linked COFs.[40] Further investigations into the effects of temperature indicated that lower temperatures do not foster the self-healing process of the framework. While it is feasible to attain an ordered structure under such conditions, achieving a highly ordered structure proves challenging (Table S2 and Fig. S1†). Examination of the influence of monomer concentration revealed minimal impact on the crystallinity of the material, indicating its potential suitability for scale-up synthesis (Table S3 and Fig. S2†). Moreover, increasing the equivalents of the PA monomer manifests a nuanced yet positive impact on crystallinity, and the presence of excess PA does not restrict the formation process of the material (Table S4 and Fig. S3†).

To further elucidate the formation process, a time-dependent transformation experiment was performed. Suspensions containing the monomers PA and TA in *o*-DCB were subjected to heating at 120 °C for varying durations of 0.5, 1, 2, 6, and 12 hours, respectively. As illustrated in Fig. 2a, PXRD analysis reveals the presence of characteristic peaks corresponding to COF–TA–PA ($2\theta = 11.1°$ and 15.6°) within 0.5 hour, indicating the formation of crystalline materials. Upon prolonging the reaction time to 1 hour, a slight enhancement in the intensity of the XRD diffraction peaks was observed, while extending the reaction duration to 12 or even 72 hours did not yield a notable enhancement in the intensity of the primary diffraction peak (Fig. S4†), indicating that the framework had been established within the initial 1 hour period. Their Fourier transform infrared (FT-IR) spectra obtained at different conversion times displayed negligible changes during the 1 hour conversion process (Fig. 2b and Table S5†), thus demonstrating the consistency of their chemical composition. Additionally, nitrogen sorption experiments were conducted to assess their surface areas. As shown in Fig. S5 and S6,† their BET surface areas of the material obtained after a 1 hour reaction were nearly twice as high as those obtained after 0.5 hours. Moreover, there was only a slight increase in the BET surface area with prolonged reaction durations. The aforementioned findings indicate that aminal-linked COF–TA–PA exhibits excellent solvent compatibility, and promising scalability, enabling rapid synthesis within a timeframe as short as 1 hour.

The FT-IR spectra of COF–TA–PA indicate the absence of C(=O)–H (2803 and 2756 cm^{-1} for TA), C=O (1687 cm^{-1} for TA), and N–H (3217 cm^{-1} for PA) vibrations, suggesting a significant degree of polymerization by the near-complete consumption of TA and PA (Fig. S7†). Moreover, the identification of vibration peak attributed to CH–N bonds at 1103 cm^{-1} provides evidence supporting the formation of aminal-linked COF.[43] Furthermore, the absence of a vibration peak corresponding to C=N suggests the absence of imine bonds in the resultant material. The solid-state ^{13}C cross-polarization magic-angle-spinning nuclear magnetic resonance (CP/MAS NMR) spectra of COF–TA–PA provide additional evidence supporting the formation of aminal units, which is indicated by the resonance signals observed at 88 ppm (Fig. S8†). X-ray photoelectron spectroscopy (XPS) analysis further confirmed the structure of COF–TA–PA, which

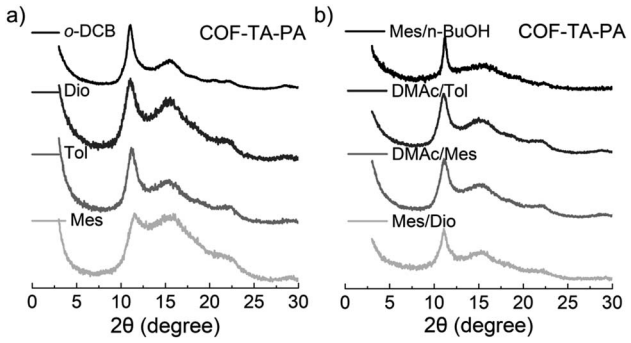

Fig. 1 PXRD patterns of COF–TA–PA obtained under different solvents.

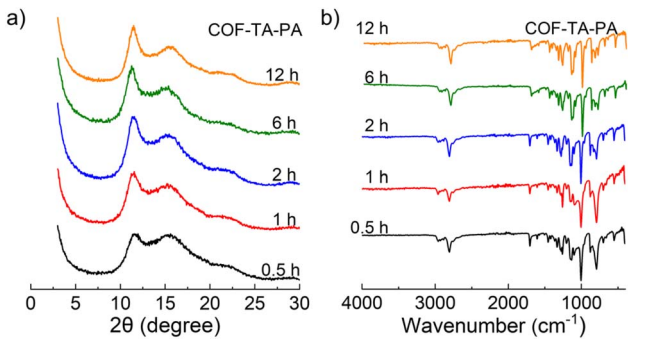

Fig. 2 (a) PXRD patterns and (b) FT-IR spectra of COF–TA–PA obtained during different reaction times.

showed a single peak at 398.78 eV (N 1s), corresponding to the aminal C–N bond (Fig. S9†).

To elucidate the adaptability of this linkage, an additional aminal-linked COF, denoted as COF–BDA–PA, was synthesized (Scheme 1). First, 4,4′-biphenyldicarboxaldehyde (BDA) and PA underwent reaction within five different solvent systems, thereby demonstrating their adeptness in yielding the target COF structures characterized by significant crystallinity (Table S6 and Fig. S10†). The preferred solvent system is *o*-DCB, aligning consistently with the synthesis of COF–TA–PA. Additionally, a time-dependent transformation experiment was conducted, and their PXRD analysis showed characteristic peaks corresponding to COF–BDA–PA (2θ = 7.3° and 10.4°) emerging within 0.5 hours indicative of crystalline structure formation (Fig. S11†). With the extension of the reaction period to 1 hour, crystalline COF materials were observed. This observation was substantiated by the FT-IR spectrum (Fig. S12†), consequently affirming the outstanding synthesis efficiency of aminal-linked COFs.

The FT-IR, solid-state ^{13}C CP/MAS NMR, and XPS (Fig. S13–S15 and Table S7†) spectra for COF–BDA–PA also confirmed the formation of an aminal-linked framework, which is similar to COF–TA–PA. The elemental analyses conducted on COF–TA–PA and COF–BDA–PA revealed their C, H, and N contents in proximity with the corresponding theoretical values calculated from anticipated polymerization products (see Experimental section). The thermogravimetric analyses (TGA) demonstrated that COF–TA–PA and COF–BDA–PA exhibited thermally stable up to 255 and 228 °C, respectively (Fig. S16†). Field emission scanning electron microscopy (SEM) and transmission electron microscopy (TEM) analyses revealed that both COF–TA–PA and COF–BDA–PA manifested nanoparticle aggregate morphology with the size of about 50 nm (Fig. S17 and S18†).

The crystallographic characteristics of the as-prepared aminal-linked COFs were investigated utilizing powder X-ray diffraction (XRD), as illustrated in Fig. 3. The PXRD patterns exhibited discernible peaks at 2θ = 11.1° (200), 15.6° (101), 18.3° (030), and 20.6° (220) for COF–TA–PA, and at 2θ = 7.3° (010), 9.8° (1–10), 10.4° (100), 14.5° (020), 16.0° (011), and 19.6° (2−20) for COF–BDA–PA. Structure modelling and Pawley refinement, conducted using Materials Studio software, facilitated the generation of their plausible structures characterized by 2D AA stacking and AB stacking. A comparative assessment between the experimental PXRD patterns (Fig. 3 black) and simulated ones revealed a closer correspondence of experimental diffraction peaks with simulated patterns featuring AA stacking (Fig. 3 orange), as opposed to those exhibiting AB stacking (Fig. 3 purple). The disparity plots (Fig. 3 gray) suggested that the refined PXRD patterns (Fig. 3 red) aligned well with the experimental ones. Pawley refinements were carried out to determine the unit cell parameters. For COF–TA–PA, the refined parameters were established as follows: a = 17.41 Å, b = 16.23 Å, c = 5.86 Å, $\alpha = \beta = 90°$, and $\gamma = 120°$, yielding residuals R_p = 2.13% and R_{wp} = 2.70% (Tables S9 and S11†). Likewise, for COF–BDA–PA, the parameters were determined as a = 9.79 Å, b = 13.96 Å, c = 6.45 Å, $\alpha = \beta = 90°$, and $\gamma = 114.6°$, resulting in residuals R_p = 3.73% and R_{wp} = 4.75% (Tables S10 and S12†). These parameters closely align with the corresponding structural models, thereby serving as additional validation for the successful synthesis of aminal-linked COFs utilizing AA stacking, consistent with prior research findings.[40]

Nitrogen sorption measurements were conducted at 77 K to assess the porosity of aminal-linked COFs. As shown in Fig. 4 (blue line), the sorption profiles of COF–TA–PA and COF–BDA–PA exhibit a type I isotherm with a rapid N_2 uptake at the low relative pressure range P/P_0 < 0.05, which is characteristic of microporous materials. Their BET surface areas were calculated based on the N_2 adsorption data in the range of P/P_0 between 0.05 and 0.30 (Fig. S19†). The BET surface areas were calculated to be 1076 and 1088 $m^2\ g^{-1}$, while the total pore volumes (at P/P_0 = 0.98) were measured to be 0.86 and 1.11 $cm^3\ g^{-1}$ for COF–TA–PA and COF–BDA–PA, respectively. The pore size distributions (PSDs), calculated by quenched solid density functional theory (QSDFT), were evaluated to be 0.57 and 0.59 nm for COF–TA–PA and COF–BDA–PA, respectively (Fig. 4c and d). These values are

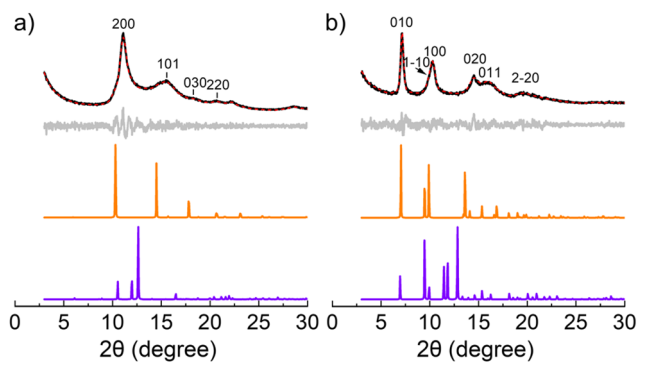

Fig. 3 Experimental (black) and Pawley-refined (red) PXRD patterns, difference plot between the observed and refined patterns (light grey), AA stacking patterns (orange), and AB stacking patterns (purple) for (a) COF–TA–PA and (b) COF–BDA–PA.

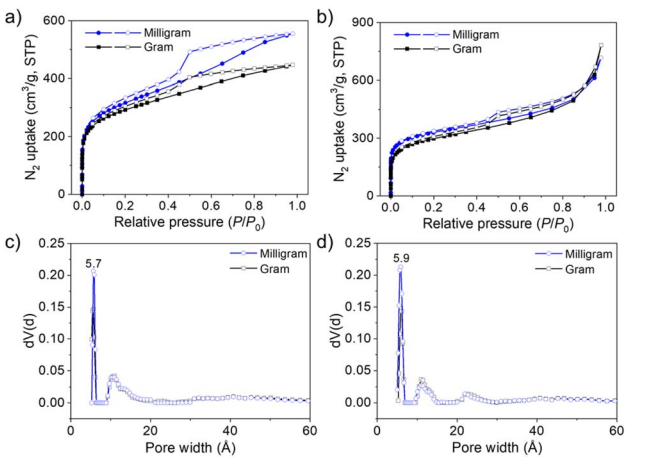

Fig. 4 (a and b) N_2 sorption isotherm curves of (a) COF–TA–PA and (b) COF–BDA–PA. (c and d) PSD profiles of (c) COF–TA–PA and (d) COF–BDA–PA. The blue line is milligram-scale synthesis, the black line is gram-scale synthesis.

in good agreement with the theoretical frameworks with AA stacking (0.56 nm for COF–TA–PA, 0.69 nm for COF–BDA–PA, as estimated by Zeo^{++} calculations) (Fig. S20†).[44,45] Other minor peak distributions indicate that defects exist in the obtained COFs.

The scale-up synthesis of COFs (see Experimental section) and simultaneous characterization were performed to study the feasibility of scale-up synthesis. Experimental results show that their crystallinity is well preserved (Fig. S21†) and their BET surface area and PSD are only slightly reduced compared to samples prepared at the milligram scale (Fig. 4 black line).

The aminal-linked COFs obtained in this study showcase microporous channels and possess a heightened nitrogen content, thus establishing their prominence as noteworthy candidates for gas adsorption applications. Methane (CH_4) is a crucial component of natural gas, serving as a primary energy source for electricity generation, heating systems, and industrial processes.[46,47] However, the presence of carbon dioxide (CO_2) in natural gas diminishes its calorific efficacy and engenders corrosion within pipelines, thereby augmenting both economic expenditures and safety hazards.[48] Purification processes are imperative to ensure that the methane extracted from natural gas is of high quality, maximizing its energy potential. Hence, the separation of CO_2/CH_4 to improve the purity of CH_4 is of significant importance for the development and application of nature technologies. In this study, we conducted an investigation to assess the performance of aminal-linked COFs in the separation of CO_2/CH_4. The single-component sorption isotherms of CO_2 and CH_4 were first collected (Fig. S22†). At 298 K, COF–TA–PA shows capacities of 33 and 12 cm^3 g^{-1} for CO_2 and CH_4 uptake (Fig. 5a), respectively. Conversely, the corresponding values of COF–BDA–PA are 53 and 19 cm^3 g^{-1}, respectively. These two aminal-linked COFs did not exhibit excellent CO_2 adsorption capacity as expected, possibly attributed to the smaller pore size. The isosteric heat of adsorption (Q_{st}), calculated by the Clausius–Clapeyron equation, suggested that COF–TA–PA had a higher binding affinity for CO_2 (29.27 kJ mol^{-1}) than for CH_4 (17.47 kJ mol^{-1}), while the binding affinity of CO_2 and CH_4 for COF–BDA–PA was 18.24 and 6.51 kJ mol^{-1}, respectively (Fig. S23†).

We assessed the CO_2/CH_4 adsorption selectivity for the CO_2/CH_4 (v/v = 50/50) mixed gas using the ideal adsorbed solution theory (IAST) by fitting CO_2 and CH_4 adsorption isotherms at pressures up to 100 kPa at 273 and 298 K (Fig. S24 and Table S8†). The CO_2/CH_4 selectivity of COF–TA–PA is determined to be 3, which is almost the same as that of COF–BDA–PA (Fig. 5b). Then we performed the experimental breakthrough studies for aminal-linked COFs at room temperature and pressure, in which the CO_2/CH_4 (v/v = 50/50) gas mixtures flowed over a packed column of the activated COF samples with the flow rate of 2 mL min^{-1}. As shown in Fig. 5c and d, CH_4 was eluted from the column first and reached high purity with no CO_2 detected. CO_2 was preferentially adsorbed by aminal-linked COFs and broke through the column after a substantial delay (16 min for COF–TA–PA and 19 min for COF–BDA–PA). The adsorbents exhibit facile regeneration through purging with helium at 298 K owing to their relatively low Q_{st} values. Recycling tests did not evidence a notable decline in separation efficacy.

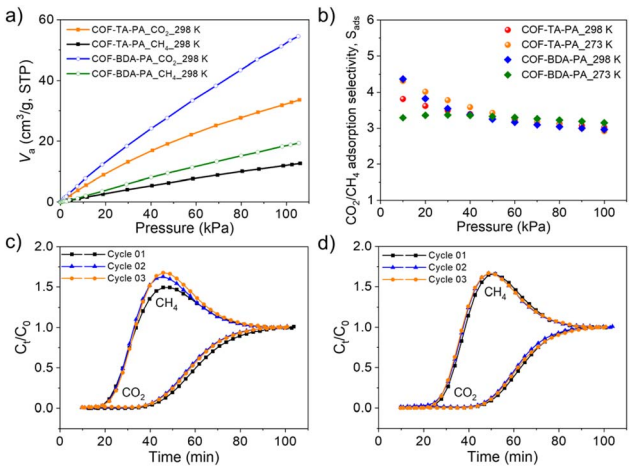

Fig. 5 (a) CO_2/CH_4 adsorption isotherms of COF–TA–PA and COF–BDA–PA at 298 K. (b) IAST selectivity (CO_2/CH_4 = 1 : 1, v/v) of COF–TA–PA and COF–BDA–PA at 273 and 298 K. Cycling breakthrough curves of (c) COF–TA–PA and (d) COF–BDA–PA for the CO_2/CH_4 (v/v = 50/50) mixed gas at 298 K with a flow rate of 2 mL min^{-1}.

Conclusions

In summary, we have deeply studied the characteristics of COFs based on aminal linkages and achieved an expedited synthesis of COFs within a one-hour duration. Two aminal-linked COFs exhibit excellent solvent compatibility and scalability, possess ultra-microporous channels, and have structures with high nitrogen content. Those unique properties highlight the application potential of these materials in gas separation and purification, and experiment results have verified that the material has a certain separation ability for CO_2/CH_4. Moreover, this study offers a novel pathway for the expeditious synthesis of large-scale, high-quality COF materials, which will facilitate the investigation of practical applications of this unique type of aminal-linked COFs.

Data availability

Data for this article, including scheme and figures are available at **https://doi.org/10.1039/d4ra02505a**. The data supporting this article have been included as part of the ESI.†

Author contributions

X. Feng and X. Han conceived and supervised the project. J. Yang and X. Han carried out the experiment. J. Yang, X. Han and X. Feng wrote and revised the manuscript.

Conflicts of interest

The authors declare no competing interests.

Acknowledgements

This work was supported by the National Natural Science Foundation of China (Grant No. 21922502 and 22171022), National Key Research and Development Program of China (2020YFB1506300), Natural Science Foundation of Shandong Province (Grant No. ZR2021QB170), China Postdoctoral Science Foundation (Grant No. 2021M700416), Beijing Municipal Science and Technology Commission No. Z211100002421013, Beijing Institute of Technology Research Fund Program and Analysis and Testing Center of Beijing Institute of Technology.

Notes and references

1 A. P. Côté, A. I. Benin, N. W. Ockwig, M. O'Keeffe, A. J. Matzger and O. M. Yaghi, *Science*, 2005, **310**, 1166–1170.
2 X. Feng, X. Ding and D. Jiang, *Chem. Soc. Rev.*, 2012, **41**, 6010–6022.
3 R. Liu, K. T. Tan, Y. Gong, Y. Chen, Z. Li, S. Xie, T. He, Z. Lu, H. Yang and D. Jiang, *Chem. Soc. Rev.*, 2021, **50**, 120–242.
4 C. J. Doonan, D. J. Tranchemontagne, T. G. Glover, J. R. Hunt and O. M. Yaghi, *Nat. Chem.*, 2010, **2**, 235–238.
5 L. Zhu and Y.-B. Zhang, *Molecules*, 2017, **22**, 1149–1178.
6 X. H. Han, K. Gong, X. Huang, J. W. Yang, X. Feng, J. Xie and B. Wang, *Angew. Chem., Int. Ed.*, 2022, **61**, e202202912.
7 Z. Wang, S. Zhang, Y. Chen, Z. Zhang and S. Ma, *Chem. Soc. Rev.*, 2020, **49**, 708–735.
8 Z. Kang, Y. Peng, Y. Qian, D. Yuan, M. A. Addicoat, T. Heine, Z. Hu, L. Tee, Z. Guo and D. Zhao, *Chem. Mater.*, 2016, **28**, 1277–1285.
9 S.-Y. Ding, J. Gao, Q. Wang, Y. Zhang, W.-G. Song, C.-Y. Su and W. Wang, *J. Am. Chem. Soc.*, 2011, **133**, 19816–19822.
10 P. Pachfule, A. Acharjya, J. Roeser, T. Langenhahn, M. Schwarze, R. Schomacker, A. Thomas and J. Schmidt, *J. Am. Chem. Soc.*, 2018, **140**, 1423–1427.
11 J. Guo and D. Jiang, *ACS Cent. Sci.*, 2020, **6**, 869–879.
12 Y. Yusran, H. Li, X. Guan, Q. Fang and S. Qiu, *EnergyChem*, 2020, **2**, 100035.
13 S. S. A. Shah, M. S. Javed, T. Najam, M. A. Nazir, A. U. Rehman, A. Rauf, M. Sohail, F. Verpoort and S. J. Bao, *Mater. Today*, 2023, **67**, 229–255.
14 X. Liu, D. Huang, C. Lai, G. Zeng, L. Qin, H. Wang, H. Yi, B. Li, S. Liu, M. Zhang, R. Deng, Y. Fu, L. Li, W. Xue and S. Chen, *Chem. Soc. Rev.*, 2019, **48**, 5266–5302.
15 L. Wei, T. Sun, Z. Shi, Z. Xu, W. Wen, S. Jiang, Y. Zhao, Y. Ma and Y.-B. Zhang, *Nat. Commun.*, 2022, **13**, 7936.
16 Q. Fang, J. Wang, S. Gu, R. B. Kaspar, Z. Zhuang, J. Zheng, H. Guo, S. Qiu and Y. Yan, *J. Am. Chem. Soc.*, 2015, **137**, 8352–8355.
17 S. Das, T. Sekine, H. Mabuchi, T. Irie, J. Sakai, Y. Zhao, Q. Fang and Y. Negishi, *ACS Appl. Mater. Interfaces*, 2022, **14**, 48045–48051.
18 M.-X. Wu and Y.-W. Yang, *Chin. Chem. Lett.*, 2017, **28**, 1135–1143.
19 C. R. DeBlase, K. E. Silberstein, T. Thanh-Tam, H. D. Abruna and W. R. Dichtel, *J. Am. Chem. Soc.*, 2013, **135**, 16821–16824.
20 F. Xu, H. Xu, X. Chen, D. Wu, Y. Wu, H. Liu, C. Gu, R. Fu and D. Jiang, *Angew. Chem., Int. Ed.*, 2015, **54**, 6814–6818.
21 J. Li, X. Jing, Q. Li, S. Li, X. Gao, X. Feng and B. Wang, *Chem. Soc. Rev.*, 2020, **49**, 3565–3604.
22 S. J. Lyle, P. J. Waller and O. M. Yaghi, *Trends Chem.*, 2019, **1**, 172–184.
23 X. Han, R.-R. Liang, Z.-B. Zhou, Q.-Y. Qi and X. Zhao, *Chem. Commun.*, 2023, **59**, 2461–2464.
24 T. Ma, E. A. Kapustin, S. X. Yin, L. Liang, Z. Zhou, J. Niu, L. H. Li, Y. Wang, J. Su, J. Li, X. Wang, W. D. Wang, W. Wang, J. Sun and O. M. Yaghi, *Science*, 2018, **361**, 48–52.
25 M. S. Lohse and T. Bein, *Adv. Funct. Mater.*, 2018, **28**, 1705553.
26 N. L. Campbell, R. Clowes, L. K. Ritchie and A. I. Cooper, *Chem. Mater.*, 2009, **21**, 204–206.
27 W. Ji, Y.-S. Guo, H.-M. Xie, X. Wang, X. Jiang and D.-S. Guo, *J. Hazard. Mater.*, 2020, **397**, 122793.
28 S.-T. Yang, J. Kim, H.-Y. Cho, S. Kim and W.-S. Ahn, *RSC Adv.*, 2012, **2**, 10179–10181.
29 J. Yoo, S. Lee, S. Hirata, C. Kim, C. K. Lee, T. Shiraki, N. Nakashima and J. K. Shim, *Chem. Lett.*, 2015, **44**, 560–562.
30 B. P. Biswal, S. Chandra, S. Kandambeth, B. Lukose, T. Heine and R. Banerjee, *J. Am. Chem. Soc.*, 2013, **135**, 5328–5331.
31 N. Brown, Z. Alsudairy, R. Behera, F. Akram, K. C. Chen, K. Smith-Petty, B. Motley, S. Williams, W. Y. Huang, C. Ingram and X. L. Li, *Green Chem.*, 2023, **25**, 6287–6296.
32 S. Kim, C. Park, M. Lee, I. Song, J. Kim, M. Lee, J. Jung, Y. Kim, H. Lim and H. C. Choi, *Adv. Funct. Mater.*, 2017, **27**, 1700925.
33 M. Zhang, J. Chen, S. Zhang, X. Zhou, L. He, M. V. Sheridan, M. Yuan, M. Zhang, L. Chen, X. Dai, F. Ma, J. Wang, J. Hu, G. Wu, X. Kong, R. Zhou, T. E. Albrecht-Schmitt, Z. Chai and S. Wang, *J. Am. Chem. Soc.*, 2020, **142**, 9169–9174.
34 X. Li, C. Yang, B. Sun, S. Cai, Z. Chen, Y. Lv, J. Zhang and Y. Liu, *J. Mater. Chem. A*, 2020, **8**, 16045–16060.
35 M. Matsumoto, R. R. Dasari, W. Ji, C. H. Feriante, T. C. Parker, S. R. Marder and W. R. Dichtel, *J. Am. Chem. Soc.*, 2017, **139**, 4999–5002.
36 J. Lu, F. Lin, Q. Wen, Q.-Y. Qi, J.-Q. Xu and X. Zhao, *New J. Chem.*, 2019, **43**, 6116–6120.
37 S.-Y. Jiang, S.-X. Gan, X. Zhang, H. Li, Q.-Y. Qi, F.-Z. Cui, J. Lu and X. Zhao, *J. Am. Chem. Soc.*, 2019, **141**, 14981–14986.
38 R. W. Layer, *Chem. Rev.*, 1963, **63**, 489–510.
39 Q. Y. Wang, J. Liu, M. Cao, J. H. Hu, R. Pang, S. Wang, M. Asad, Y. L. Wei and S. Q. Zang, *Angew. Chem., Int. Ed.*, 2022, **61**, e202207130.
40 H. Yun, M. Kang, D. W. Kang, H. Kim, J. H. Choe, S. Y. Kim and C. S. Hong, *Small*, 2023, **19**, e2303640.
41 P. Peng, L. Shi, F. Huo, S. Zhang, C. Mi, Y. Cheng and Z. Xiang, *ACS Nano*, 2019, **13**, 878–884.
42 G. Greczynski and L. Hultman, *Appl. Surf. Sci.*, 2022, **606**, 154855.
43 M. K. Dezfuli and M. R. Saidi, *Phosphorus, Sulfur Silicon Relat. Elem.*, 2004, **179**, 89–96.
44 R. L. Martin, B. Smit and M. Haranczyk, *J. Chem. Inf. Model.*, 2012, **52**, 308–318.

45 T. F. Willems, C. H. Rycroft, M. Kazi, J. C. Meza and M. Haranczyk, *Microporous Mesoporous Mater.*, 2012, **149**, 134–141.
46 T. Yan, Y. Lan, M. Tong and C. Zhong, *ACS Sustainable Chem. Eng.*, 2019, **7**, 1220–1227.
47 P. Hu, H. Wang, C. Xiong, H. Liu, J. Han, J. Zhou, Z. Zhao, Y. Wang and H. Ji, *ACS Sustain. Chem. Eng.*, 2021, **9**, 15897–15907.
48 H. Tan, Q. Chen, T. Chen, Z. Wei and H. Liu, *Chem. Eng. J.*, 2020, **391**, 123521.